# Elastic properties of Pu metal and Pu-Ga alloys

Per Söderlind, Alex Landa, and J. E. Klepeis
*Lawrence Livermore National Laboratory, Livermore, California 94550, USA*

Y. Suzuki and A. Migliori
*Los Alamos National Laboratory, Los Alamos, New Mexico 87545, USA*

(Received 23 March 2010; revised manuscript received 3 June 2010; published 17 June 2010)

We present elastic properties, theoretical and experimental, of Pu metal and Pu-Ga ($\delta$) alloys together with *ab initio* equilibrium equation of state for these systems. For the theoretical treatment we employ density-functional theory in conjunction with spin-orbit coupling and orbital polarization for the metal and coherent-potential approximation for the alloys. Pu and Pu-Ga alloys are also investigated experimentally using resonant ultrasound spectroscopy. We show that orbital correlations become more important proceeding from $\alpha \rightarrow \beta \rightarrow \gamma$ plutonium, thus suggesting increasing $f$-electron correlation and a corresponding softening of the elastic moduli. For the $\delta$-Pu-Ga alloys we find a softening with larger Ga content, i.e., atomic volume, bulk modulus, and elastic constants imply a weakened chemical bonding with addition of Ga. Our measurements confirm qualitatively the theory but uncertainties remain when comparing the model with experiments.

DOI: 10.1103/PhysRevB.81.224110 PACS number(s): 71.15.Mb, 71.15.Rf, 71.27.+a, 75.10.Lp

## I. INTRODUCTION

Plutonium metal and alloys provide great challenges for theoreticians and experimentalists alike. Theoretically, complex crystal and electronic structures combined with electron correlations greater than most metals and strong relativistic effects make Pu very difficult to tackle. On the experimental side, Pu is chemically toxic and radioactive, causing safety and other regulatory concerns that make it demanding to work with. Consequently, theory and experiment have been able to highlight some facets of this material but not reveal the complete physical picture.

Elasticity constitutes one of the core properties of any material, one that is paramount for engineering issues. It is related to strength and other mechanical properties. On a fundamental material science level, elastic moduli provide a very detailed representation of the chemical bonding and thus reflects characteristics of the electronic structure. The latter is particularly important when evaluating and contrasting different theoretical models. In the case of Pu (and presumably Pu containing alloys) dynamical mean-field theory[1] is claimed to describe the electron-correlation effects, while on the other hand, total-energy calculations obtained from density-functional theory (DFT) appears consistent with many ground-state properties.[2–4] Here we are comparing DFT adiabatic single-crystal elastic constants with resonant ultrasound spectroscopy (RUS) polycrystal elastic moduli in an effort to validate the DFT model for Pu and $\delta$-Pu-Ga alloys electronic structure. We note that single crystal and polycrystal bulk moduli are the same within 2% while single-crystal Kroner average of shear moduli also agree with similar accuracy.[5] Our study is complementary to other investigations[6] of the electronic structure, many of which were reviewed recently by Moore and van der Laan.[7]

We are applying DFT to examine equilibrium equation of state and single-crystal elastic constants of the six known phases of Pu metal $(\alpha, \beta, \gamma, \delta, \delta', \epsilon)$ and $\delta$-Pu-Ga alloy (0–10 at. % Ga). In Fig. 1 we show the Pu phases and indicate their crystal type and number of independent elastic constants. In parallel with the theory we are presenting resonant ultrasound spectroscopy measurements on polycrystal $\alpha$, $\beta$, and $\gamma$ plutonium as well as some $\delta$-Pu-Ga alloys. The experimental data are important for understanding materials properties but they are also essential in corroborating the DFT approach and any other theoretical model. For semi-empirical techniques the development of interatomic potentials can be constrained by the presented experimental elastic constants and in some cases, where data are missing, our DFT predictions.

In Sec. II we describe technical details of the computations including our theoretical model for the studied Pu systems. This is followed by Sec. III in which we briefly describe our elastic-moduli measurements. Next, calculated crystal stabilities and equilibrium equation-of-state data of the various phases are presented in Sec. IV. Our theoretical

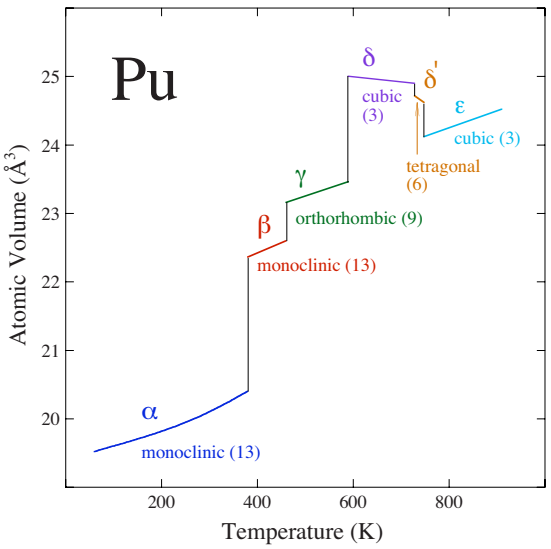


FIG. 1. (Color online) The experimental phase diagram of Pu. The type of crystal and number of independent elastic constants are indicated.

 

and experimental results for the elastic moduli are given in Sec. V and we provide concluding remarks in Sec. VI.

## II. COMPUTATIONAL

The electronic structure and total energy are obtained from density-functional calculations which require the crystal geometry and the atomic number (94 for Pu and 31 for Ga). As is dictated by DFT, the electron exchange and correlation energy functionals and associated potentials have to be assumed and we use the so-called generalized gradient approximation (GGA) for this purpose.[8]

For pure Pu in its complex phases we are adopting an all-electron technique that has proven to be robust for the actinides in the past.[9] The linear muffin-tin orbitals (LMTO) method does not constrain the shapes of the charge density or potential and the method is thus referred to as a full-potential LMTO (FPLMTO) method.[10]

Electron correlations play an important role in Pu and Pu-rich alloys. Within the framework of DFT it has been shown that calculations including spin polarization, spin-orbit (SO) coupling, and orbital polarization (OP) in conjunction with GGA can produce realistic total energies for all phases[3] but the high-temperature body-centered-cubic (bcc) $\epsilon$ phase. We have argued that antiferromagnetic order for the $\alpha$, $\beta$, and $\gamma$ phases and magnetic disorder for the higher temperature phases best represent plutonium within the assumptions of the DFT model.[11,12] Following this recipe we calculate the total energy as a function of strain and extract the elastic moduli. For $\alpha$-Pu the effects of orbital polarization on the elastic properties were suggested to be small[13] when they were evaluated at the same atomic volume, corresponding to the equilibrium of the SO+OP treatment. Nevertheless, the elasticity of all phases are evaluated at the equilibrium volume of the full (SO+OP) theory for both the SO and SO+OP approximations.

Spin-orbit coupling is implemented in a first-order variational procedure[14] for the valence $d$ and $f$ states, as was done previously,[2] and for the core states the fully relativistic Dirac equation is solved. The orbital polarization is accomplished as described in detail.[15] The energy of the orbitals with the spin, orbital, and magnetic quantum numbers $(\sigma,l,m_l)$ are shifted an amount proportional to $L_\sigma m_l$. Here $L_\sigma$ is the total orbital moment from electrons with spin $\sigma$. This self-consistent parameter-free technique attempts to generalize Hund's second rule for an atom to the condensed matter and enhances the separation of the $m_l$ orbitals caused by the spin-orbit interaction. Hence, the OP can be viewed as an amplification of the SO.

The axial ratios of all lower symmetry phases ($\alpha$ and $\beta$ monoclinic, $\gamma$ orthorhombic, and $\delta'$ tetragonal) are varied (optimized) to produce the lowest total energy. Internal coordinates are kept fixed at their measured values.[16] The monoclinic phases have 13, the orthorhombic 9, tetragonal 6, and cubic phases 3 independent elastic coefficients that correspond to specific strains of the lattice. Small strains ($\sim$max 1–2 %) are applied and the total-energy response fitted to a fourth-order polynomial allowing for the extraction of the second-order coefficient that is proportional to the corresponding elastic modulus. All applicable strains and equations for this scheme were presented earlier.[13,17] We are ignoring lattice relaxation during the distortions due to technical limitations of our computations. In the case of $\alpha$ uranium this simplification was determined to be acceptable[17] but could possibly influence the calculated elastic coefficients.

The calculations of random substitutional alloys ($\delta$-Pu-Ga) are best performed within the coherent-potential approximation (CPA).[18] This procedure also conveniently allows for the treatment of magnetic disorder which otherwise is modeled by a supercell (special quasirandom structure) as before.[11] The CPA is here applied in an identical manner as in our previous study of pure $\delta$-Pu (Ref. 19) within the exact MTO (EMTO) method.[20] The EMTO calculations are performed using scalar relativistic, spin-polarized, Green's-function technique based on the improved screened Korringa-Kohn-Rostoker method for which the electron potential and density are precise enough to be used for the small lattice distortions associated with elastic constants. The details are the same as for pure $\delta$-Pu (Ref. 19) but here we study the $\delta$-Pu-Ga alloy for concentrations 2, 4, 6, 8, and 10 at. % Ga.

## III. EXPERIMENTAL

The elastic moduli are determined from measurements of the resonance frequencies using a RUS (Refs. 21–23) system constructed entirely of ceramics, metals, and other inorganic materials to preclude deleterious radiolytic interactions. The system can operate between 1.8 and 700 K. Several approaches to temperature control are taken in the presented results but the primary measurements are made in He atmosphere. Temperature is controlled to about 100 mK with an accuracy better than 2%. The specific shapes of the samples are mostly responsible for errors in the densities and elastic moduli. Therefore, considerable care is taken to ensure square and parallel shapes of the samples with dimensional errors less than 5 $\mu$m. A detailed description of the processing, impurity levels, error sources, and experimental technique has been presented previously for pure Pu (Ref. 24) and the Pu-Ga (2.36 at. %) alloy.[25]

## IV. CRYSTAL STABILITIES AND EQUILIBRIUM EQUATION OF STATE

Before examining the elastic properties we study the crystal stabilities and equilibrium equation-of-state properties of the Pu phases and the $\delta$-Pu-Ga alloys. We begin with $\alpha$-Pu for which the theory is reproducing the details of the monoclinic structure[16] very well as pointed out in our previous publications.[13,26] The calculations of the elastic constants for the monoclinic ($P2_1/m$) $\alpha$-Pu thus assumes the measured data for axial ratios, monoclinic angle, and atomic positions at the theoretical equilibrium volume 20.3 Å$^3$.

The $\beta$ phase is also monoclinic with space group $B2/m$ and 17 atoms in the primitive unit cell with 34 atoms per unit cell as described in the Pu handbook.[16] Due to the complexity to fully relax all structural parameters, particularly in the

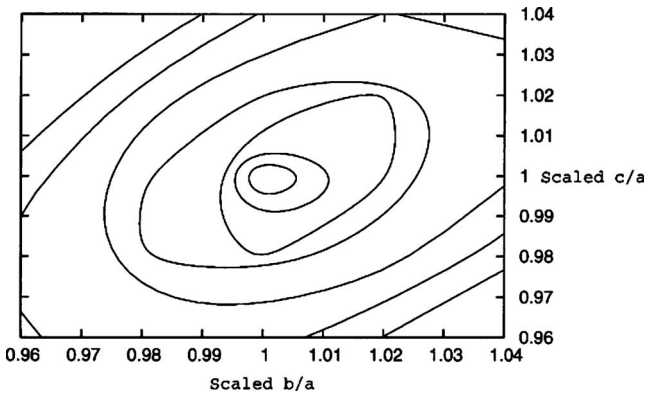


FIG. 2. Equitotal-energy curves as a function of axial $b/a$ and $c/a$ ratios for $\beta$-Pu obtained from the fully correlated (SO+OP) treatment. Here the axial ratios are scaled with their measured (Ref. 16) values. The plot shows a minimum close to (1.0, 1.0) which represents the measured axial ratios. The first five energy contours are separated by 0.02 mRy/atom with a 0.1 mRy/atom separation for the remaining ones.

context of an all-electron methodology, we are limiting ourselves to only calculate the total energy as a function of $b/a$ and $c/a$ axial ratios at the equilibrium volume obtained from computations using the measured[16] geometry. In Fig. 2 we show the total-energy contours of $\beta$-Pu as a function of $b/a$ and $c/a$ axial ratios at the theoretical equilibrium volume (23.1 Å$^3$). Here the axial ratios have been scaled with their experimental[16] values ($b/a=1.127$ and $c/a=0.847$). The total energies are obtained from our full treatment of electron correlations (SO+OP) and the figure shows a minimum in the energy landscape at (1.0, 1.0), i.e., the calculations are perfectly reproducing the measured ratios. For comparison we also show, in Fig. 3, a similar plot at the same atomic volume but without spin polarization, spin-orbit coupling, and orbital polarization. In this case there is no energy minimum anywhere close to the axial ratios observed for $\beta$-Pu. In contrast, there is a downhill slope in energy toward much

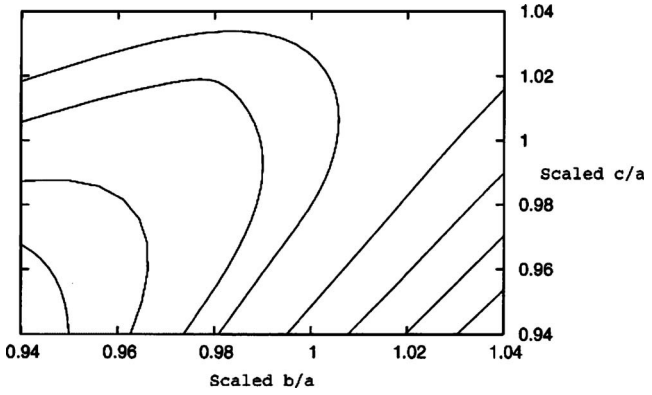


FIG. 3. Same as Fig. 2 but here the calculations do not include spin polarization, spin-orbit coupling, or orbital polarization. The plot shows a drop in total energy for axial ratios smaller than 94% of the experimental (Ref. 16) values. The actual total-energy minimum for this simplified model lies outside the plotted ranges. The first five energy contours are separated by 0.25 mRy/atom with a 0.5 mRy/atom separation for the remaining ones.

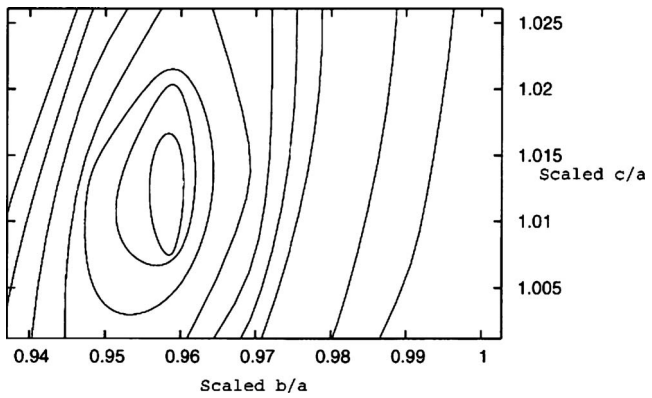


FIG. 4. Same as Fig. 2 but here for $\gamma$-Pu. The plot shows a minimum close to (0.96, 1.01) which is relatively close to the measured (1.0, 1.0) axial ratios (Ref. 16). The first four energy contours are separated by 0.01 mRy/atom and 0.02 mRy for the remaining ones.

smaller axial ratios suggesting a structural instability of $\beta$-Pu. Obviously, electron correlations are very important for the structural stability of $\beta$-Pu and must be considered in any realistic model for the elastic constants. Spin polarization plays a role but is likely not as essential as SO and OP. Recent calculations[27] for $\delta$-Pu show that when SO and OP are both included the effect of spin polarization is largely diminished.

The $\gamma$ phase is orthorhombic with space group *Fddd* and eight atoms per primitive unit cell that is also present[28,29] in compressed americium (AmIII) close to 10 GPa. In this face-centered-orthorhombic structure the atomic coordinates are, contrary to the $\beta$ phase, bound by symmetry. Full relaxation of $\gamma$-Pu is therefore easier to accomplish and it suffices to optimize the axial ratios at a given atomic volume. In Fig. 4 we show a total-energy contour plot at the theoretical equilibrium volume (23.8 Å$^3$) of $\gamma$-Pu similar to that of $\beta$-Pu in Fig. 2. As before, the axial ratios have been scaled with measured data[16] ($b/a=1.826$ and $c/a=3.217$). The energy minimum occurs at about (0.96, 1.01) suggesting that the $c/a$ ratio is very good while the $b/a$ is slightly underestimated (4%). DFT without the aforementioned electronic-correlation effects is completely unable to model this phase (not shown), a fact that has been discussed in the literature previously.[30,31]

Both the $\delta$ and $\epsilon$ phases are cubic with structures entirely defined by their face-centered-cubic (fcc) and body-centered-cubic symmetries. Between them there is a small pocket of stability for the $\delta'$ tetragonal ($I4/mmm$) phase, see Fig. 1. Our calculated equilibrium volume for this phase is 24.7 Å$^3$ and the optimized axial ratio is about 3.5% larger than the observed[16] (1.329), see Fig. 5.

Thus, in addition to plausible total energies and atomic densities,[3] our DFT model suggests structural stability for all Pu phases, except the $\epsilon$ phase (see below), with rather good crystal parameters as well. In Sec. V we shall apply small strains to the optimized structure of each phase for evaluation of the elastic moduli.

Next, we summarize our equilibrium equation-of-state properties for pure Pu in its six known phases together with experimental data taken from the literature. In Table I we

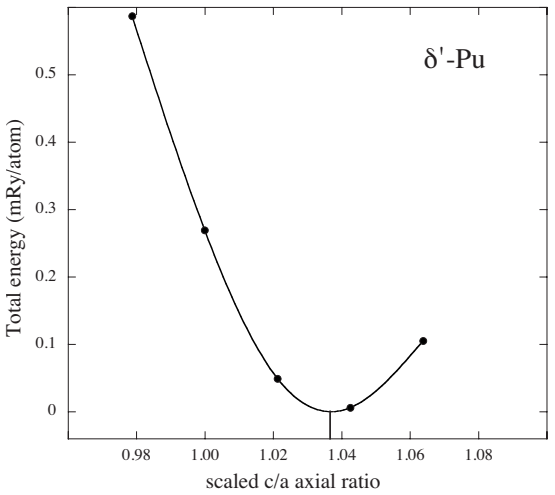


FIG. 5. Total energy as a function of $c/a$ axial ratio for $\delta'$-Pu. The axial ratio has been scaled with its measured value (Ref. 16). The calculations overestimate the axial ratio slightly (3.5%).

show atomic volumes ($V$) and bulk moduli ($B$), obtained from Murnaghan[32] fits to our total energies, for the fully correlated treatment (SO+OP), and with spin-orbit coupling and spin polarization only (SO). For the more limited treatment, SO, we also evaluate $B$ at the equilibrium volume for the full theory ($B_{fix}$). The calculation of $B_{fix}$ will allow for a more consistent comparison because the influence of different equilibrium volumes is removed and the same approach

TABLE I. Present FPLMTO (SO and SO+OP) and EMTO results together with experimental data (Refs. 16, 37, and 38). $B_{fix}$ is the bulk modulus evaluated at the equilibrium volume corresponding to the full electron-correlation treatment (SO+OP).

| Phase | Method | $V$ | $B$ | $B_{fix}$ |
|---|---|---|---|---|
| $\alpha$ | SO | 19.0 | 59 | 25 |
| $\alpha$ | SO+OP | 20.3 | 45 | 45 |
| $\alpha$ | Expt. | 20.0–20.4 | 37–66 | |
| $\beta$ | SO | 22.0 | 41 | 33 |
| $\beta$ | SO+OP | 23.1 | 37 | 37 |
| $\beta$ | Expt. | 22.7 | 34.3 | |
| $\gamma$ | SO | 22.7 | 38 | 30 |
| $\gamma$ | SO+OP | 23.8 | 32 | 32 |
| $\gamma$ | Expt. | 23.5 | 25.7 | |
| $\delta$ | SO | 24.2 | 46 | 39 |
| $\delta$ | SO+OP | 24.9 | 41 | 41 |
| $\delta$ | EMTO | 25.5 | 39.6 | 44.2 |
| $\delta$ | Expt. | 25.0 | 29–30 | |
| $\delta'$ | SO | 24.2 | 41 | 38 |
| $\delta'$ | SO+OP | 24.7 | 44 | 44 |
| $\delta'$ | Expt. | 24.8 | | |
| $\epsilon$ | SO | 23.9 | 21 | 20 |
| $\epsilon$ | SO+OP | 24.6 | 23 | 23 |
| $\epsilon$ | EMTO | 26.6 | 29.7 | 32 |
| $\epsilon$ | Expt. | 24.4 | | |

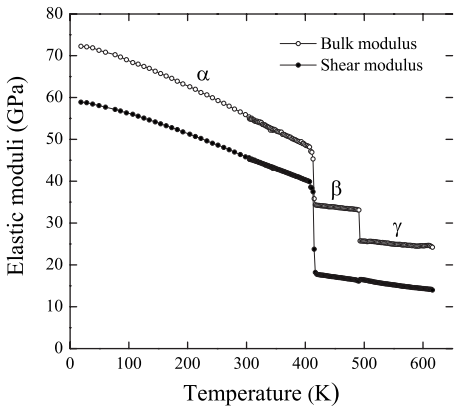


FIG. 6. Our measured temperature dependence, with error bars, for the (B) bulk and (G) shear moduli for $\beta$ and $\gamma$ plutonium.

is adopted for the elastic constants below (Sec. V). Clearly, electron correlation plays an important role because the difference between the SO and SO+OP equilibrium volumes is substantial for all phases. Generally, the bulk modulus ap-

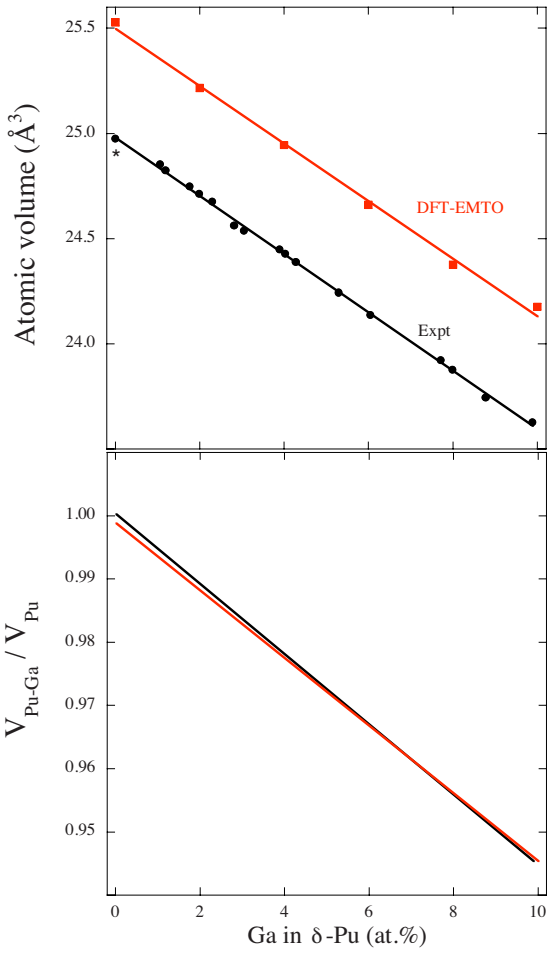


FIG. 7. (Color online) Upper panel: EMTO atomic volume for $\delta$-Pu-Ga as a function of Ga content together with experimental (Ref. 33) data. The FPLMTO result is marked with a star. Lower panel: EMTO and experimental atomic volumes scaled with their respective $\delta$-Pu values. Notice the essentially identical dependence on Ga content between our calculations and measurements.

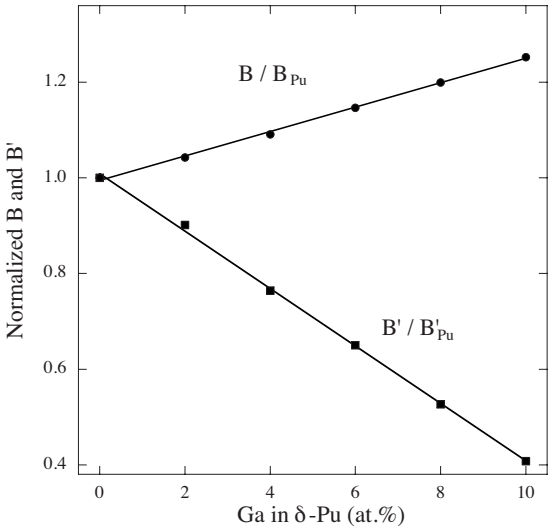


FIG. 8. EMTO $B$ and $B'$ as functions of Ga content in $\delta$-Pu-Ga alloy. Both quantities depend linearly on the amount of Ga.

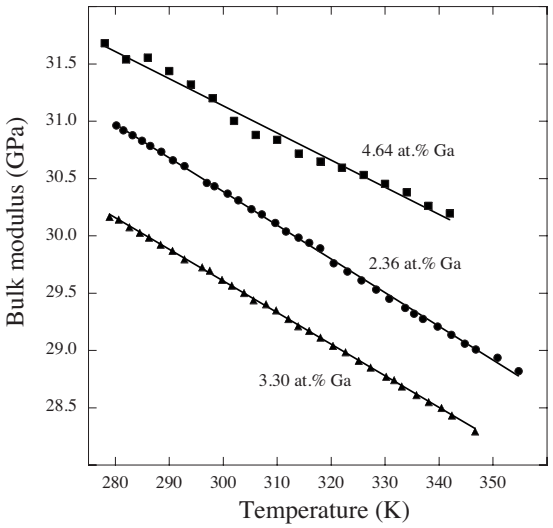


FIG. 9. Present RUS measurements of the bulk modulus as a function of temperature for the 2.36, 3.30, and 4.64 at. % Ga specific $\delta$-Pu-Ga alloys.

pears to be less dependent on the two theoretical treatments particularly when evaluated at the same (SO+OP) volume ($B_{fix}$). For all phases, Table I reveals that DFT predicts atomic volumes very close to experimental data and reasonable bulk moduli as well. One cannot, however, expect perfect agreement because temperature effects are not accounted for in the theory. This is demonstrated in Fig. 6 where we plot with error bars our measured $B$ and shear modulus ($G$, see more below) for $\beta$-Pu (~430–480 K) and $\gamma$-Pu (~480–620 K).

The $\delta$-Pu-Ga alloy system has been modeled in analogy with pure $\delta$-Pu as a magnetically disordered material and with the random substitutional alloy treated within the CPA. Although founded on the same fundamental DFT, with GGA for the exchange and correlation functionals, the CPA is here implemented in EMTO with no spin-orbit coupling and with shape approximations of charge density and electron potentials that are not present in the FPLMTO calculations. Consequently, there are some minor differences in the obtained data for $\delta$-Pu between the two methods, see Table I. The principal purpose of our EMTO-CPA calculations, however, is to investigate the influence of gallium in $\delta$-Pu. In Fig. 7 we show in the upper panel the atomic volume as a function of gallium content in $\delta$-Pu together with measured[33] data. The EMTO method predicts volumes about 2% greater than experiments (and FPLMTO) for pure $\delta$-Pu but the Ga-concentration dependence appears to be very similar to the experimental data. In the lower panel of Fig. 7 we illustrate this by plotting the scaled volume, $\frac{V_{\text{Pu-Ga}}}{V_{\text{Pu}}}$, as a function of atomic percent Ga. The volume depends linearly with Ga concentration in this studied interval where theory and experiment essentially coincide.

The bulk modulus and its pressure derivative, $B'$, also depends linearly on Ga content in our calculations. Figure 8 displays these properties and notice here that $B$ increases and $B'$ decreases in a linear fashion. For three concentrations (2.36, 3.30, and 4.64 at. % Ga) we measure the temperature dependence of the bulk modulus, shown in Fig. 9. At any given temperature there is an increase in the bulk modulus between 2.36 and 4.64 at. % Ga in $\delta$-Pu. At 300 K the relative increase is about 2.3% while our calculations (Fig. 8) suggest a larger increase (5.5%). Interestingly, our measurements for the 3.30 at. % Ga alloy have a lower bulk modulus and this is not reproduced by our theory.

The calculated pressure derivative of the bulk modulus is responsive to the Ga content, see Fig. 8, which is consistent with the fact that the thermal expansion is very sensitive to alloying. Our calculations do not, however, predict a negative $B'$ necessary for the anomalous negative thermal expansion.

## V. ELASTIC CONSTANTS

The single-crystal elastic constants for $\alpha$-Pu were recently calculated[13] and we follow the same procedure here to also compute these for the $\beta$, $\gamma$, $\delta$, and $\delta'$ phases of Pu. For the high-temperature $\epsilon$ phase our disordered magnetic model[11,12] predicts a negative tetragonal shear constant and thus no mechanical stability. We speculate that phonon anharmonicity and entropy, not accounted for in the present model, are promoting its stability before melt.

Although it was suggested[13] that electron correlation, in terms of orbital polarization, has an insignificant influence on

TABLE II. $\alpha$-Pu elastic constants in gigapascal at 20.3 Å$^3$.

| Method | $c_{11}$ | $c_{22}$ | $c_{33}$ | $c_{44}$ | $c_{55}$ | $c_{66}$ | $c_{12}$ | $c_{13}$ | $c_{23}$ | $c_{15}$ | $c_{25}$ | $c_{35}$ | $c_{46}$ |
|---|---|---|---|---|---|---|---|---|---|---|---|---|---|
| SO | 120 | 109 | 86.2 | 43.4 | 50.6 | 43.7 | −9.30 | 1.10 | −11.5 | 22.1 | 20.2 | 21.9 | −0.25 |
| SO+OP | 121 | 116 | 93.7 | 46.6 | 55.6 | 41.5 | −5.2 | 2.9 | −8.3 | 23.2 | 23.8 | 21.6 | −2.3 |

TABLE III. $\beta$-Pu elastic constants in gigapascal at 23.1 Å$^3$.

| Method | $c_{11}$ | $c_{22}$ | $c_{33}$ | $c_{44}$ | $c_{55}$ | $c_{66}$ | $c_{12}$ | $c_{13}$ | $c_{23}$ | $c_{15}$ | $c_{25}$ | $c_{35}$ | $c_{46}$ |
|---|---|---|---|---|---|---|---|---|---|---|---|---|---|
| SO | 75.1 | 63.1 | 64.3 | 35.8 | 21.4 | 26.5 | 22.0 | 20.6 | 18.1 | 21.3 | 21.4 | 21.8 | −0.30 |
| SO+OP | 75.4 | 64.4 | 65.1 | 32.2 | 22.4 | 27.2 | 27.0 | 20.6 | 23.1 | 20.6 | 21.5 | 19.4 | −0.95 |

the moduli for $\alpha$-Pu we choose here to investigate its importance in detail for all Pu phases. In Tables II and III we present the monoclinic elastic constants for the $\alpha$ and $\beta$ phases, respectively. First we notice that orbital polarization has a minor, but non-negligible, influence on the moduli for the $\alpha$ and $\beta$ phases. The six $c_{ii}$ components have straightforward interpretations, the three first, $c_{11}$, $c_{22}$, and $c_{33}$, correspond to strains in the $x$, $y$, and $z$ directions, respectively. The next three, $c_{44}$, $c_{55}$, and $c_{66}$, are related to strains causing changes in the angles between the axes. Focusing on the $c_{ii}$'s, which are more intuitive than the others, we find that they are significantly smaller for $\beta$ than $\alpha$ plutonium. Because they scale inversely with the atomic volume[13] a reduction is expected following the volume expansion associated with the $\alpha \rightarrow \beta$ transition. The difference in volume suggests a decrease on the order of 12% while the actual reduction is considerably greater (see below).

The succeeding phase in Pu (Fig. 1) is the orthorhombic $\gamma$-Pu. Due to the higher crystal symmetry in $\gamma$, compared to $\alpha$ and $\beta$ plutonium, fewer elastic constants are independent. Still, nine strains are needed to obtain all of them and the procedure was outlined in detail in our previous investigation of $\alpha$-U.[17] The results are listed in Table IV and they show that orbital polarization is more important for the elasticity in the $\gamma$ phase compared to that of $\alpha$ and $\beta$ plutonium. In this sense, electron correlation appears to be stronger in $\gamma$-Pu than the lower temperature phases. In Fig. 10 we plot the average $c_{ii}$ for $\alpha$, $\beta$, and $\gamma$ plutonium. In this figure we also display the results when the average $c_{ii}$ for the $\alpha$ phase is being scaled corresponding to the lower densities (greater atomic volumes) of the $\beta$ and $\gamma$ phases. Clearly, the average $c_{ii}$ decreases more strongly with the phase transitions than a simple volume scaling suggests. The reduced magnitude of the elastic constants are thus driven not only by changes in the atomic density but also by phase-specific alterations in the character of the chemical bonds as one proceeds through the $\alpha \rightarrow \beta \rightarrow \gamma$ transitions. These variations in the electronic structure can be interpreted as indicative of $5f$-electron localization or increasing electron correlation.

The next transition takes plutonium to the cubic $\delta$ phase. Although $\delta$-Pu is stable only in a narrow range at relatively high temperatures, it can be stabilized to room temperature and below by adding small amounts of an appropriate metal. One often-used additive is gallium which therefore motivates our study on the $\delta$-Pu-Ga alloy system. First, however, we address unalloyed $\delta$-Pu. As mentioned, a cubic system has only three independent elastic constants ($c_{11}$, $c_{12}$, and $c_{44}$). As is a common practice when calculating elastic constants for cubic metals, we have chosen to compute the tetragonal shear constant, $c' = \frac{c_{11}-c_{12}}{2}$ together with $c_{44}$ and separate $c_{11}$ and $c_{12}$ by using the bulk modulus (Table I) and the relationship $B = \frac{c_{11}+2c_{12}}{3}$.

The theoretical elastic constants are collected and compared to single-crystal data on $\delta$-Pu in Table V. First we realize that FPLMTO and EMTO results are not identical. Our previous report on $\delta$-Pu (Ref. 19) recognized this as well and it is expected when the methods adopt distinct approximations. The present $c_{44}$ is also slightly lower than earlier data[19] and more accurate because we apply smaller strains (EMTO) and use more $k$ points for the band structure (FPLMTO). Compared to single-crystal data, both methods overestimate $c_{11}$ somewhat while $c_{12}$ and $c_{44}$ are relatively close. Also, $c_{44}$ for the EMTO calculation appears too high. Unless fortunate cancellations of errors occur in the computations, we expect the FPLMTO to be more accurate than EMTO which does not include spin-orbit coupling and orbital polarization, even though the latter evidently has a relatively small influence, see Table I. In addition, the nonspherical parts of charge density and potentials are treated differently between the techniques which may cause minor disparities in the elastic constants.

With increasing temperature, Pu returns once again to a lower symmetry phase, i.e., the tetragonal $\delta'$. Elastic constants have not been measured for this phase that is only stable in a small sliver of the phase diagram (Fig. 1). Nevertheless, for completeness, we also present our predictions for $\delta'$-Pu in Table VI. The tetragonal symmetry is higher than that of the orthorhombic and six elastic constants are independent. The equations relating strains to the orthorhombic moduli[17] can be used observing the fact that $c_{22}=c_{11}$, $c_{55}=c_{44}$, and $c_{23}=c_{13}$. Table VI suggests that OP has a small but non-negligible influence on the $c_{ij}$'s similar to the other phases. For the SO+OP treatment $c_{33} \simeq c_{11}$ and $c_{66} \simeq c_{44}$ which may suggest a chemical bonding akin to higher (cubic) symmetry even though $c_{12} \neq c_{13}$.

The final phase before melting, $\epsilon$-Pu, as we have alluded to, does not have a positive tetragonal shear constant $c'$ and is therefore mechanically unstable. This fact was already

TABLE IV. $\gamma$-Pu elastic constants in gigapascal at 23.8 Å$^3$.

| Method | $c_{11}$ | $c_{22}$ | $c_{33}$ | $c_{44}$ | $c_{55}$ | $c_{66}$ | $c_{12}$ | $c_{13}$ | $c_{23}$ |
|---|---|---|---|---|---|---|---|---|---|
| SO | 91.1 | 67.2 | 74.5 | 28.6 | 14.1 | 27.5 | 8.80 | 22.9 | 16.0 |
| SO+OP | 81.0 | 63.7 | 70.5 | 21.6 | 11.9 | 21.7 | 3.15 | 22.6 | 22.6 |

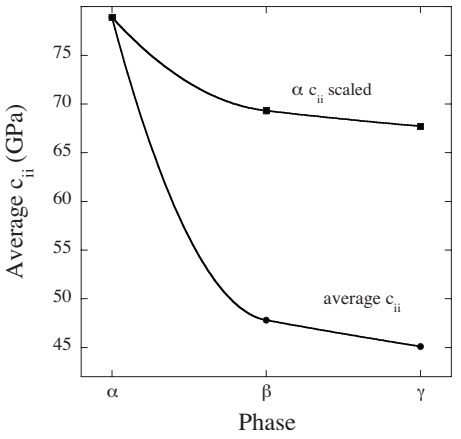


FIG. 10. Average $c_{ii}$ (solid circles) for $\alpha$, $\beta$, and $\gamma$ plutonium. Solid squares show the average $c_{ii}$ for $\alpha$-Pu scaled with the equilibrium volume of the respective phases (see text). Solid lines are guides to the eye only.

observed[11] in the calculated tetragonal (Bain) transformation path that displayed a local maximum for the bcc ($\epsilon$) phase. It was also noted[3] that the total energy for this phase is too high to be less than 200 K above the $\delta$ phase. Both these failures of the model, we believe, are related to our low-temperature treatment of this high-temperature phase for which entropy, not included in our model, is absolutely essential. A similar situation occurs for many metals including Ti, Zr, and Hf for which a solution, based on a self-consistent *ab initio* lattice-dynamics method, has recently been presented.[34]

Let us now return to the $\delta$ phase focusing on the Ga-stabilized system. In Fig. 11 we plot our calculated $c'$ and $c_{44}$ for $\delta$-Pu-Ga up to 10 at. % Ga. Both moduli soften with increasing Ga content while the anisotropy ratio ($\frac{c_{44}}{c'}$), shown in the inset, reaches a maximum $\sim$9 for 6 at. % Ga. For pure Pu, ultrasonic[35] and x-ray[36] measure this ratio to be 7.1 and 6.3, respectively. Incidentally, our SO+OP FPLMTO calculations for $\delta$-Pu (Table V) suggest a more isotropic system with $\frac{c_{44}}{c'} \sim 2$. The stark contrast between the two sets of calculations of this ratio lies in the fact that one overestimates $c'$ and the other $c_{44}$.

Next, we attempt to compare our calculated single-crystal elastic constants with experimental data obtained from polycrystal samples. The comparison necessitates an averaging procedure for the single-crystal results. There are many ways of approximating an effective polycrystal modulus from single-crystal data and the Kroner average for cubic systems,

TABLE V. FPLMTO (SO and SO+OP) and EMTO $\delta$-Pu elastic constants in gigapascal at 24.9 Å$^3$ and 25.5 Å$^3$, respectively. Experimental data (Ref. 33) is for single-crystal $\delta$-Pu.

| Method | $c_{11}$ | $c_{12}$ | $c_{44}$ |
|---|---|---|---|
| SO | 61.7 | 27.7 | 35.0 |
| SO+OP | 65.0 | 29.0 | 38.0 |
| EMTO | 50.1 | 34.4 | 65.3 |
| Expt. | 36 | 26 | 31 |

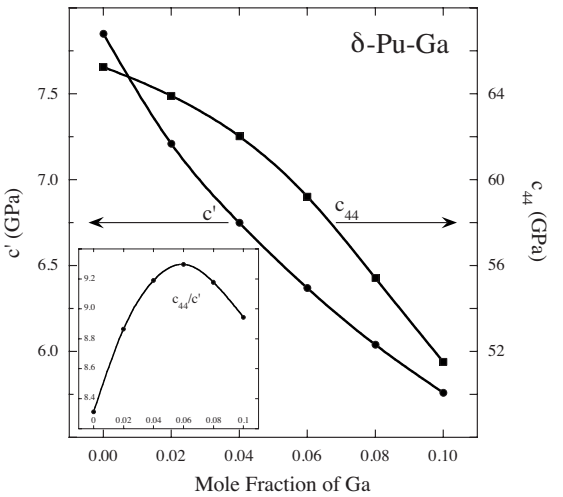


FIG. 11. EMTO $c'$ and $c_{44}$ elastic constants as functions of Ga content. The inset shows the corresponding anisotropy ratio $c_{44}/c'$. Solid lines are guides to the eye only.

often the best compromise, produces excellent agreement between single-crystal and polycrystal data. Currently, however, this scheme is not available for the lower symmetry phases. It is not our intention here to explore averaging techniques but rather in a consistent fashion relate our theoretical results for all Pu phases and the $\delta$-Pu-Ga system to our polycrystal data. As in our previous paper on $\alpha$-Pu (Ref. 13) we simply adopt the Voigt expressions for calculating the shear and bulk modulus which we then use to obtain $\tilde{c}_{11}$ through

$$B = \tilde{c}_{11} - \frac{4G}{3}, \tag{1}$$

where $\tilde{c}_{11}$ is calculated from the measured sound speed through the relationship $v_1 = \sqrt{\frac{\tilde{c}_{11}}{\rho}}$. The Voigt upper bounds for the bulk ($B_V$) and shear ($G_V$) moduli are, for noncubic lattices,

$$B_V = \frac{1}{9}[c_{11} + c_{22} + c_{33} + 2(c_{12} + c_{13} + c_{23})] \tag{2}$$

and

$$G_V = \frac{1}{15}[c_{11} + c_{22} + c_{33} + 3(c_{44} + c_{55} + c_{66}) - (c_{12} + c_{13} + c_{23})], \tag{3}$$

respectively. Applying Eqs. (1)–(3) together with our calculated single crystal $c_{ij}$, presented above, we fill the entries in Table VII. The RUS data entered here cover the $\alpha$, $\beta$, and $\gamma$ phases together with room temperature (300 K) $\delta$-Pu alloyed

TABLE VI. $\delta'$-Pu elastic constants in gigapascal at 24.7 Å$^3$.

| Method | $c_{11}$ | $c_{33}$ | $c_{44}$ | $c_{66}$ | $c_{12}$ | $c_{13}$ |
|---|---|---|---|---|---|---|
| SO | 61.0 | 49.3 | 39.1 | 31.3 | 35.2 | 25.6 |
| SO+OP | 64.7 | 62.0 | 42.1 | 42.2 | 43.2 | 29.6 |

TABLE VII. Presently calculated Voigt averages of bulk and shear moduli ($B_V$, $G_V$, and $\tilde{c}_{11}$, see text) together with present RUS and literature data (Refs. 16, 37, and 38). Data in parenthesis are present RUS values extrapolated to zero temperature. All in units of gigapascal. SO and SO+OP (FPLMTO) data are calculated at the equilibrium volume of the SO+OP treatment while EMTO results for $\delta$-Pu are evaluated at the EMTO equilibrium volume (25.5 Å$^3$).

| Phase | Method | $B_V$ | $G_V$ | $\tilde{c}_{11}$ |
|---|---|---|---|---|
| $\alpha$ | SO | 30.6 | 49.9 | 97.1 |
| $\alpha$ | SO+OP | 34.4 | 51.3 | 102.8 |
| $\alpha$ | Expt.(poly) | 37–54.4 (72) | 43.5–43.7 (59) | 104.6–112.8 (116.2) |
| $\beta$ | SO | 36.0 | 26.2 | 70.9 |
| $\beta$ | SO+OP | 38.5 | 25.3 | 72.2 |
| $\beta$ | Expt.(poly) | 34.4 (41) | 18.2 (26) | 58.7 (75.7) |
| $\gamma$ | SO | 36.5 | 26.4 | 71.7 |
| $\gamma$ | SO+OP | 34.6 | 22.2 | 64.2 |
| $\gamma$ | Expt.(poly) | 25.7 (31) | 16.5 (27) | 47.7 (67) |
| $\delta$ | SO | 39.0 | 27.8 | 76.0 |
| $\delta$ | SO+OP | 41.0 | 30.6 | 81.8 |
| $\delta$ | EMTO | 39.6 | 42.3 | 96.0 |
| $\delta$ | Expt.(poly) | 29.7 (38) | 16.2 (20) | 51.3 (64.7) |
| $\delta$ | Expt. (single) | 29.0 | 21.0 | 57.0 |
| $\delta'$ | SO | 38.2 | 26.8 | 73.9 |
| $\delta'$ | SO+OP | 44.0 | 31.4 | 85.9 |

with 2.36 at. % Ga. The latter approximates unalloyed $\delta$-Pu well because the elastic properties depend only very weakly on small Ga concentrations for $\delta$-Pu in our RUS measurements (not shown). No RUS data is collected for the $\delta'$ or $\epsilon$ phases. Elastic moduli at the lowest temperature that stabilizes each phase, see Fig. 6, are compiled in Table VII. Notice that theory and experimental data compare relatively well for $\alpha$, $\beta$, and $\gamma$ taking into account that $G_V$ is an upper bound for $G$. Experimental data extrapolated to zero temperature are quite close to theory for the $\beta$, $\gamma$, and $\delta$ phases whereas for the $\alpha$ phase the room-temperature data agree better.

Our calculated $\delta$-Pu moduli can be directly compared with the single-crystal data and they agree fairly well as discussed above. As with the polycrystal data, we expect the agreement to improve considerably for data extrapolated to zero temperature (not available). A similar level of accuracy is expected also for $\delta'$ plutonium but the answer has to wait until the measurements have been done.

## VI. CONCLUSION

We report the first theoretical single-crystal elastic constants for all phases of Pu metal, excluding the $\epsilon$ phase, and also for the $\delta$-Pu-Ga alloy system. Accompanying these are RUS measurements for polycrystal $\alpha$, $\beta$, $\gamma$, and Ga-stabilized $\delta$ plutonium. All Pu polymorphs, except $\epsilon$, are predicted by theory to be mechanically stable having crystal geometries close to their true observed structures. Also, the magnitudes of the DFT elastic constants appear to be similar to what is obtained from the RUS measurements, particularly for the $\alpha$, $\beta$, and $\gamma$ phases. From this and the fact that DFT energies are consistent with the phase diagram[3] one must conclude that the electronic structure for Pu is well described by the DFT model and the aforementioned electron correlations.

The elastic properties $\delta$-Pu (and presumably $\delta'$-Pu) agree somewhat less favorably with single-crystal or polycrystal RUS data and it may suggest that electron-correlation effects are treated more approximately than for the lower temperature phases. Alternatively, entropies not accounted for may play a greater role at higher temperatures as we have already suggested above for the $\epsilon$ phase. Either way, key features of the $\delta$-Pu chemical bonding are reproduced by theory including a small tetragonal shear constant ($c'$), a larger anisotropy ratio ($c_{44}/c'$) than most metals, good lattice constant, and a good bulk modulus.

We predict a linear behavior, as a function of Ga concentration, for the atomic volume, bulk modulus, and the pressure derivative of the bulk modulus for the $\delta$-Pu-Ga system. The decrease in the atomic volume with Ga content is in excellent agreement with experiment. For $B$, our RUS data indicate a substantial increase between 2.36 and 4.64 at. % Ga, in accord with our alloy calculations, whereas for the 3.30 at. % Ga alloy $B$ has a minimum in the RUS analysis that is not predicted by theory. The volume behavior (Fig. 7) is somewhat surprising because on one hand adding Ga contracts the $\delta$-Pu volume closer to that of $\alpha$-Pu while on the other it stabilizes the $\delta$ relative to the $\alpha$ phase. Our DFT

model correctly captures this interesting result, which is simply due to the fact that Ga has a smaller size than Pu in the fcc phase.

Uncertainties remain when theoretical results are related to experimental data. (i) No temperature dependence is accounted for in the theory. (ii) The comparison between single-crystal and polycrystal moduli is imperfect due to the necessary averaging procedure involved. (iii) Relaxation effects are ignored both when calculating the equation-of-state properties (Table I) and for the elastic moduli (Tables II–VI).

## ACKNOWLEDGMENTS

This work performed under the auspices of the U.S. Department of Energy by Lawrence Livermore National Laboratory under Contract No. DE-AC52-07NA27344 and Los Alamos National Laboratory in the National High Magnetic Field Laboratory. This work was also supported by the U.S. National Nuclear Security Administration under Grant No. 20070013, the National Science Foundation under Grant No. DMR-0654118, and the State of Florida.

[1] A. Georges, G. Kotliar, W. Krauth, and W. Rozenberg, Rev. Mod. Phys. **68**, 13 (1996); G. Kotliar, S. Y. Savrasov, K. Haule, V. S. Oudovenko, O. Parcollet, and C. A. Marianetti, *ibid.* **78**, 865 (2006); A. B. Shick and V. A. Gubanov, Europhys. Lett. **69**, 588 (2005); L. V. Pourovskii, M. I. Katsnelson, A. I. Lichtenstein, L. Havela, T. Gouder, F. Wastin, A. B. Shick, V. Drchal, and G. H. Lander, *ibid.* **74**, 479 (2006).

[2] P. Söderlind, Europhys. Lett. **55**, 525 (2001).

[3] P. Söderlind and B. Sadigh, Phys. Rev. Lett. **92**, 185702 (2004).

[4] G. Roberts, A. Pasturel, and B. Siberchicot, J. Phys.: Condens. Matter **15**, 8377 (2003); Europhys. Lett. **71**, 412 (2005).

[5] A. Migliori, H. Ledbetter, A. C. Lawson, A. P. Ramirez, D. A. Miller, J. B. Betts, M. Ramos, and J. C. Lashley, Phys. Rev. B **73**, 052101 (2006).

[6] G. van der Laan, K. T. Moore, J. G. Tobin, B. W. Chung, M. A. Wall, and A. J. Schwartz, Phys. Rev. Lett. **93**, 097401 (2004); J. G. Tobin, K. T. Moore, B. W. Chung, M. A. Wall, A. J. Schwartz, G. van der Laan, and A. L. Kutepov, Phys. Rev. B **72**, 085109 (2005); K. T. Moore, G. van der Laan, R. G. Haire, M. A. Wall, and A. J. Schwartz, *ibid.* **73**, 033109 (2006); K. T. Moore, G. van der Laan, M. A. Wall, A. J. Schwartz, and R. G. Haire, *ibid.* **76**, 073105 (2007); J. G. Tobin, P. Söderlind, A. Landa, K. T. Moore, A. J. Schwartz, B. W. Chung, M. A. Wall, J. M. Wills, R. G. Haire, and A. L. Kutepov, J. Phys.: Condens. Matter **20**, 125204 (2008); M. T. Butterfield, K. T. Moore, G. van der Laan, M. A. Wall, and R. G. Haire, Phys. Rev. B **77**, 113109 (2008).

[7] K. T. Moore and G. van der Laan, Rev. Mod. Phys. **81**, 235 (2009).

[8] J. P. Perdew, J. A. Chevary, S. H. Vosko, K. A. Jackson, M. R. Pederson, D. J. Singh, and C. Fiolhais, Phys. Rev. B **46**, 6671 (1992).

[9] P. Söderlind, Adv. Phys. **47**, 959 (1998).

[10] J. M. Wills, O. Eriksson, M. Alouani, and D. L. Price, in *Electronic Structure and Physical Properties of Solids*, edited by H. Dreysse (Springer-Verlag, Berlin, 1998), p. 148.

[11] P. Söderlind, A. Landa, and B. Sadigh, Phys. Rev. B **66**, 205109 (2002).

[12] A. Landa, P. Söderlind, and A. V. Ruban, J. Phys.: Condens. Matter **15**, L371 (2003).

[13] P. Söderlind and J. E. Klepeis, Phys. Rev. B **79**, 104110 (2009).

[14] O. K. Andersen, Phys. Rev. B **12**, 3060 (1975).

[15] O. Eriksson, B. Johansson, and M. S. S. Brooks, J. Phys.: Condens. Matter **1**, 4005 (1989); O. Eriksson, M. S. S. Brooks, and B. Johansson, Phys. Rev. B **41**, 9087 (1990).

[16] O. J. Wick, *Plutonium Handbook A Guide to the Technology* (Gordon and Breach, New York, 1967).

[17] P. Söderlind, Phys. Rev. B **66**, 085113 (2002).

[18] J. S. Faulkner, Prog. Mater. Sci. **27**, 1 (1982).

[19] P. Söderlind, A. Landa, B. Sadigh, L. Vitos, and A. Ruban, Phys. Rev. B **70**, 144103 (2004).

[20] L. Vitos, *Computational Quantum Mechanics for Materials Engineers: The EMTO Method and Applications* (Springer, London, 2007).

[21] A. Migliori, J. L. Sarrao, W. M. Visscher, T. M. Bell, M. Lei, Z. Fisk, and R. G. Leisure, Physica B **183**, 1 (1993).

[22] A. Migliori and J. Sarrao, *Resonant Ultrasound Spectroscopy* (Wiley-Interscience, New York, 1997).

[23] A. Migliori and J. D. Maynard, Rev. Sci. Instrum. **76**, 121301 (2005).

[24] A. Migliori, C. Pantea, H. Ledbetter, I. Stroe, J. B. Betts, J. N. Mitchell, M. Ramos, F. Freibert, D. Dooley, S. Harrington, and C. H. Mielke, J. Acoust. Soc. Am. **122**, 1994 (2007).

[25] A. Migliori, I. Mihut-Stroe, and J. B. Betts, *Actinides 2008: Basic Science, Applications, and Technology*, Material Research Society Symposium Proceedings No. 1104 (Materials Research Society, Pittsburgh, 2008), p. 193.

[26] B. Sadigh, P. Söderlind, and W. G. Wolfer, Phys. Rev. B **68**, 241101(R) (2003).

[27] P. Söderlind, Phys. Rev. B **77**, 085101 (2008).

[28] S. Heathman, R. G. Haire, T. Le Bihan, A. Lindbaum, K. Litfin, Y. Meresse, and H. Libotte, Phys. Rev. Lett. **85**, 2961 (2000); A. Lindbaum, S. Heathman, K. Litfin, Y. Meresse, R. G. Haire, T. Le Bihan, and H. Libotte, Phys. Rev. B **63**, 214101 (2001).

[29] P. Söderlind and A. Landa, Phys. Rev. B **72**, 024109 (2005).

[30] J. Bouchet, R. C. Albers, M. D. Jones, and G. Jomard, Phys. Rev. Lett. **92**, 095503 (2004).

[31] P. Söderlind, B. Sadigh, and K. T. Moore, Phys. Rev. Lett. **93**, 199601 (2004).

[32] F. D. Murnaghan, Proc. Natl. Acad. Sci. U.S.A. **30**, 244 (1944).

[33] F. H. Ellinger, C. C. Land, and V. O. Struebing, J. Nucl. Mater. **12**, 226 (1964).

[34] P. Souvatzis, O. Eriksson, M. I. Katsnelson, and S. P. Rudin, Phys. Rev. Lett. **100**, 095901 (2008).

[35] H. M. Ledbetter and R. L. Moment, Acta Metall. **24**, 891 (1976).

[36] J. Wong, M. Krisch, D. L. Farber, F. Occelli, A. J. Schwartz, T.-C. Chiang, M. Wall, C. Boro, and R. Xu, Science **301**, 1078 (2003).

[37] Ph. Faure and C. Genestier, J. Nucl. Mater. **385**, 38 (2009).

[38] A. Migliori, I. Mihut, J. B. Betts, M. Ramos, C. Mielke, C. Pantea, and D. Miller, J. Alloys Compd. **444-445**, 133 (2007).